

Energy loss of heavy ions in dense plasma. II. Nonequilibrium charge states and stopping powers

Thomas Peter and Jürgen Meyer-ter-Vehn

Max-Planck-Institut für Quantenoptik, D-8046 Garching, Federal Republic of Germany

(Received 4 June 1990)

The effective charge Z_{eff} of fast heavy ions slowing down in hot dense matter is calculated simultaneously with the stopping power dE/dx . The various ionization and recombination processes determining Z_{eff} are discussed, and corresponding rate coefficients are given; particular attention is paid to dielectronic recombination which turns out to be the dominant capture mechanism in highly ionized target material. Important results are (1) the effective charge of heavy ions passing through matter is considerably higher for fully ionized plasma than for cold target matter; (2) in contrast to stopping in cold targets, where Z_{eff} runs through a series of equilibrium charge states essentially determined by the instantaneous projectile velocity, high nonequilibrium charge states of the projectile are found in strongly ionized targets due to reduced recombination and faster stopping; (3) this causes additional range shortening, in some cases by factors 2–7, in particular for relatively low projectile energies ($E_{\text{ion}} < 2$ MeV/u) and target densities ($n < 10^{20}$ cm $^{-3}$). Typical results for Z_{eff} and dE/dx in this parameter region are presented. They are compared with recent experimental data; new experiments are proposed. Concerning applications to heavy-ion-driven inertial fusion, the described effects become relevant at the end of the range, and some illustrative cases are discussed.

I. INTRODUCTION

The stopping power dE/dx of heavy ions in matter is proportional to the square of the effective charge Z_{eff} of the projectile

$$-\frac{dE}{dx} \propto Z_{\text{eff}}^2, \quad (1)$$

at least in leading order. In the preceding paper¹ (hereafter called paper I) the plasma physics aspects of stopping heavy ions in highly ionized matter were discussed, showing that the scaling given by Eq. (1) is valid for

$$\frac{Z_{\text{eff}}}{n_e \lambda_D^3} \frac{1}{1 + v_p^3 / (k_B T / m)^{3/2}} \ll 1. \quad (2)$$

Here, n_e , T , m are density, temperature, and mass of the plasma electrons, respectively; v_p is the projectile ion velocity, and the Debye length is given by $\lambda_D = (k_B T / 4\pi n_e e^2)^{1/2}$. In paper I it was assumed that Z_{eff} is a fixed number. In this second paper, the physics determining Z_{eff} is considered.

For protons, and also for light ions of sufficient energy, Z_{eff} is equal to the nuclear charge Z_{nuc} and does not change along the stopping path. For heavy ions, however, the change of Z_{eff} plays an important role, in particular, close to the end of the range. In cold condensed matter, Z_{eff} is essentially a function of the projectile velocity v_p reflecting the fact that the ionization and recombination processes determining Z_{eff} occur on a timescale shorter than the energy loss and the charge states, therefore, evolve along a sequence of equilibrium values. Typically semiempirical formulas for $Z_{\text{eff}}(v_p)$ like the Betz formula² or the one by Nikolaev and Dmitriev³ have been

used in stopping-power calculations, even for hot ionized stopping material.^{4,5}

For highly ionized plasma targets, however, equilibrium values of Z_{eff} are often not reached. Since recombination is strongly reduced, times for relaxation of Z_{eff} and for stopping may often become comparable and the charge states proceed through sequences of nonequilibrium states. In this case one has to solve rate equations for Z_{eff} simultaneously with the equation of energy loss. This is done in the following.

The present calculations extend the pioneering work of Nardi and Zinamon⁶ who were the first to predict considerably enhanced Z_{eff} in plasma. An important point in the present paper is the inclusion of dielectronic recombination⁷ which is often the dominant recombination process in fully ionized plasma exceeding radiative electron capture and three-body recombination. The rate coefficient of the standard ionization and recombination processes are introduced in Sec. II, and corresponding equilibrium charge states are calculated for the example of iodine projectiles in hydrogen plasma and cold hydrogen gas. Dielectronic recombination is then discussed in detail in Sec. III, and effects of high density becoming important at electron densities $n_e \gtrsim 10^{20}$ cm $^{-3}$ are treated in Sec. IV. Three-body recombination and, in particular, dielectronic recombination are strongly dependent on density.

The present work is based on relatively simple atomic modeling and utilizes screened hydrogenic energies and oscillator strengths. This simplification is necessary in view of the large parameter space $\{n_e, T_e, v_p, Z_{\text{nuc}}, Z_{\text{eff}}\}$ to be covered and appears to be justified since the rate coefficients vary over many orders of magnitude as a function of Z_{eff} so that an accuracy up to a factor of 2 in

the rates appears already satisfactory.

In Sec. V, the full time-dependent rate equations are solved together with the equations for energy loss for some representative cases. Experimental data on the energy loss of heavy ions in plasma have been obtained recently,^{8–10} and a comparison with the best set of data published so far¹¹ will be given. In the experiments, a fully ionized H plasma was produced with a Z pinch, and the energy loss of 1.4-MeV/u Pb ions could be measured up to a maximum plasma density of $2.5 \times 10^{18} \text{ cm}^{-3}$. Range shortening and the effects of dielectronic recombination and nonequilibrium charge states are rather pronounced in the parameter region covered by these experiments. In applications to heavy-ion inertial-confinement fusion (ICF) ion energies and target densities are typically higher; two cases relevant to ICF (Ref. 12) are included in the discussion of Sec. V.

II. CHARGE STATES OF IONS PENETRATING PLASMA

The effective charge of a projectile ion

$$Z_{\text{eff}}(v_p, t) \equiv \sum_{Z=0}^{Z_p} Z P_Z(v_p, t) \quad (3)$$

is defined in terms of the probability P_Z of finding the ion in charge state Z ($0 \leq Z \leq Z_{\text{nuc}}$). The P_Z are normalized according to $\sum_Z P_Z = 1$. The charge-state distribution satisfies the rate equations

$$\frac{dP_Z(v_p, t)}{dt} = \sum_{Z' (\neq Z)} [\alpha(Z' \rightarrow Z) P_{Z'}(v_p, t) - \alpha(Z \rightarrow Z') P_Z(v_p, t)], \quad (4)$$

where $\alpha(Z \rightarrow Z')$ is the total rate describing the number of transitions $Z \rightarrow Z'$ per unit time. The total rate is the sum over all rates of the individual loss and capture processes ($\alpha = \sum_i \alpha_i$), which are related to the cross sections σ_i by

$$\alpha_i = \int d^3v f_i(\mathbf{v}, \mathbf{v}_p) \sigma_i(v_p) |\mathbf{v}|, \quad (5)$$

where f_i is the shifted Maxwellian distribution of the plasma electrons or ions as seen by a projectile ion moving with velocity v_p

$$f_i(\mathbf{v}, \mathbf{v}_p) = n_i \left[\frac{m_i}{2\pi k_B T_i} \right]^{3/2} e^{-(m_i/2k_B T_i)(\mathbf{v} + \mathbf{v}_p)^2}. \quad (6)$$

Here, n_i and T_i are the plasma electron or ion density and temperature, respectively. We solve the rate equations numerically taking only one-electron processes $\alpha(Z \rightarrow Z \pm 1)$ into consideration. This is a good approximation particularly for low- Z targets.²

In the following the ionization and recombination cross sections σ_i for ions moving through a plasma are summarized and compared with the cross sections in a cold target gas. We utilize the simple Slater model for the calculation of screened hydrogenlike atomic energies¹³ and oscillator strengths; a simplification that ap-

pears to be justified in view of the extensive parameter space $\{n_e, T_e, v_p, Z_{\text{nuc}}, Z_{\text{eff}}\}$ examined in this survey.

A. Ionization by Coulomb collisions with target ions or free electrons

Among the simple, semiclassical approximations describing atomic ionization the binary-encounter model (BEM) is one of the most successful schemes. Following Gryzinski¹⁴ the cross section for ionization of an electron sitting in the n th shell of the projectile ion in a collision with the target ion is given by

$$\sigma_{\text{BEM}} = \sum_n N_n \sigma_n = \sum_n N_n \pi \left[\frac{Z_t e^2}{U_n} \right]^2 G \left[\frac{v_p}{v_n} \right]. \quad (7)$$

Here, N_n is the number of electrons in the n th shell, U_n is their binding energy, and $v_n = \sqrt{2U_n/m}$ their orbital velocity. The function G accounts for the velocity matching $v_p \approx v_n$ for optimal ionization:¹⁵

$$G(V) = \frac{\alpha^{3/2}}{V^2} \left[\alpha + \frac{2}{3}(1+\beta) \ln(2.7+V) \right] \times (1-\beta)(1-\beta^{(1+V^2)}), \quad (8)$$

where $\alpha = V^2/(1+V^2)$, $\beta = 1/[4V(1+V)]$ for $V > 0.206$. For $V < 0.206$ it is $G(V) = 4V^4/15$.

In the case of a fully ionized plasma Z_t is the nuclear charge of the target ions. If there are bound electrons, the nuclear charge will be partially screened, and an effective target charge Z_t^* has to be used in Eq. (7). Depending on its velocity v_p the projectile will penetrate more or less deeply into the target atom. According to Bell¹⁶ we approximate Z_t^* as the charge within a sphere of radius $b_n = \sqrt{\sigma_n/\pi}$. Hence, the calculation of Z_t^* requires the solution of the equations

$$Z_t^*(b_n) = \frac{U_n b_n}{e^2 \sqrt{G(v_p/v_n)}}, \quad (9)$$

$$Z_t^*(b_n) = Z_t - \sum_i N_i \int_0^{b_n} d^3r |\psi_i(\mathbf{r})|^2,$$

where $\psi_i(\mathbf{r})$ is the normalized wave function of an i th shell electron. The rate for Coulomb ionization is $\alpha_{\text{BEM}} = v_p n_i \sigma_{\text{BEM}}$. The upper dashed line in Fig. 1 shows the rate coefficient for the case of an iodine beam with $v_p = 1.5\alpha c$ in a hydrogen plasma with temperature $T = 10 \text{ eV}$ and ion density $n_i = 10^{17} \text{ cm}^{-3}$. According to the Saha equation only a relative fraction of 2×10^{-6} of the electrons are bound in such a plasma.

The main difference between ionizing collisions with target ions and free electrons is the ionization edge (see lower dashed curve in Fig. 1): electrons with $v_r < v_n$ do not have enough kinetic energy for ionization of a bound electron in the n th shell. Following Lotz¹⁷ we adapt the ionization cross section in collisions with free electrons

$$\sigma_e = \sum_n N_n \sigma_n = 4 \times 10^{-14} (\text{cm eV})^2 \times \sum_n N_n \frac{\ln(E_r/U_n)}{E_r U_n} \Theta(E_r - U_n), \quad (10)$$

with the step function $\Theta(x) = (|x| + x)/2$. We approximate the relative energy between projectile ion and plasma electron by $E_r = (m/2)v_r^2 \approx (m/2)(v_p^2 + v_{th}^2)$. The rate is $\alpha_e \approx v_r n_e \sigma_e$. The edge at $I^{24+} \rightarrow I^{25+}$ in Fig. 1 corresponds to the transition from the N shell to the M shell; the electrons do not have enough energy for M -shell ionization.

B. Radiative electron capture and three-body recombination

The cross section for radiative electron capture (REC) is related to the electronic transition probability $A(n' \rightarrow n)$ between major shells $n' \rightarrow n$ in the projectile (charge state Z) with energy $E_{n'} - E_n = \hbar\omega$. In the quasi-classical approximation following Zel'dovich and Raizer:¹⁸

$$A(n' \rightarrow n) \propto \left(\frac{Z^2}{n^2} - \frac{Z^2}{n'^2} \right)^2 \left| \frac{1}{n^3} \frac{1}{n'^3} \right| \left| \frac{1}{\left(\frac{1}{n^2} - \frac{1}{n'^2} \right)} \right|. \quad (11)$$

According to Menzel and Pekeris¹⁹ the free-bound transition in the REC process can be calculated from Eq. (11) using the substitution $n' \equiv i\kappa$, where κ is the inverse velocity v of the photoelectron in units αc :

$$A(n' \rightarrow n) d\kappa \propto \frac{Z^4}{n^3} \frac{1}{\left(\frac{1}{n^2} + \frac{1}{\kappa^2} \right)} \frac{d\kappa}{\kappa^3} \propto \frac{Z^4}{n^3} \frac{1}{\left(\frac{1}{n^2} + v^2 \right)} v dv. \quad (12)$$

$A d\kappa$ is proportional to the rate of REC into the n th projectile shell $(\sigma_n v) d^3v = (\sigma_n v) 4\pi v^2 dv$. The quantitative result due to Menzel²⁰ and Spitzer²¹ is

$$\sigma_n = A \frac{v_0}{v} \frac{h\nu_0}{m_e v_r^2} \frac{g}{n^3},$$

$$\text{where } A = \frac{2^4}{3^{3/2}} \frac{he^2}{m_e^2 c^3} = 2.1 \times 10^{-22} \text{ cm}^2, \quad (13)$$

$$h\nu = \frac{1}{2} m_e v_r^2 + \frac{h\nu_0}{n^2}, \quad h\nu_0 = Z^2 \text{ Ry}.$$

g is the free-bound Gaunt factor, $g \approx 1$.

To obtain the total rate $\alpha_{REC} = v_r n_e \sigma_{REC}$ one has to

$$\sigma_{CT} = 4.1 \times 10^4 \sum_{n_i} \sum_{n_f} N_i a_{\text{eik}} \frac{(Ze^2)^2 E_i^{5/2} E_f^{3/2} E_k^4}{[E_k^2 + 2E_k(E_i + E_f) + (E_i - E_f)^2]^5}, \quad (17)$$

where E_i and E_f are the binding energies of the electron (>0) in initial and final state, respectively, Z is the charge state of the projectile, $E_k = mv_p^2/2$, and N_i the number of electrons in the shell of the target. Equation

sum from the ground state n_g (with N_{n_g} electrons) up to large quantum numbers. In the hydrogenlike approximation

$$\alpha_{REC} = \left[1 - \frac{N_{n_g}}{2n_g^2} \right] \alpha_{n_g} + \sum_{n=n_g+1}^{\infty} \alpha_n. \quad (14)$$

The quantity α_{REC} is shown in Fig. 1 as a solid curve.

In plasmas with high density the probability for a simultaneous collision of the projectile ion with two electrons increases. One of these electrons can be captured by the projectile, while the other carries away the excess energy. Zel'dovich and Raizer¹⁸ described this three-body recombination process (3BR) using a simple classical picture. They find

$$\alpha_{3BR} = \frac{2^5 \pi^2 e^{10}}{m^5} \frac{Z^3 n_e}{v_r^9} = 2.92 \times 10^{-31} \frac{\text{cm}^3}{\text{sec}} \frac{Z^3 (n_e / \text{cm}^{-3})}{(v_r / \alpha c)^9}, \quad (15)$$

which is in good agreement with the precise theory by Pitaeviskii²² and Gurevich.²³ We compare this with radiative electron capture (v_r in αc , n_e in cm^{-3}):

$$\frac{\alpha_{REC}}{\alpha_{3BR}} \approx 1.6 \times 10^{17} \frac{\frac{Z^4}{v_r^3} g n_e}{\frac{Z^3 n_e}{v_r^9} n_e} = 1.6 \times 10^{17} \frac{Z v_r^6}{n_e}. \quad (16)$$

For laboratory plasmas radiative electron capture is many orders of magnitude larger than three-body recombination. For 1.5 MeV/ u ions ($v_r = 7.75\alpha c$) the two rates are comparable only if the density is close to solid-state density (Fig. 1).

C. Capture of bound target electrons

If the target is not fully ionized a bound electron can be transferred from a target ion to the projectile [charge transfer (CT)]. Oppenheimer²⁴ and Brinkmann and Kramers²⁵ calculated the cross section (OBK theory) for this process in first Born approximation with the simple interaction potential $-e^2/r$ and unperturbed hydrogenlike wave functions (Laguerre polynomials). Following Betz² the analytic results for the cross sections can be generalized by appropriate scaling to nuclei of arbitrary charge. We use the cross section averaged over all initial (l, m) states and summed over all final (l, m) states (May's sum rule;²⁶ Betz²):

(17) contains a reduction factor a_{eik} (in the usual OBK theory $a_{\text{eik}} = 1$). To cure the deficiency of the first-order Born approximation, which neglects the interaction between target and projectile after the charge transfer and

the possibility of the target ion to recapture the electron, Eichler *et al.*²⁷ developed an eikonal theory for the calculation of the reduction factor. They showed that

$$a_{\text{eik}} = \frac{\pi\eta v_i}{\sinh(\pi\eta v_i)} \exp \left[-2\eta v_i \arctan \left(\frac{v_p/2 - \epsilon\eta}{v_i} \right) \right] \times \left[\frac{23}{48} + \left(\frac{1}{6}v_i^2 + \frac{5}{6}\epsilon \right) \eta^2 + \frac{5}{12}\epsilon^2 \eta^4 \right] \quad (18)$$

where $\eta = \alpha c/v_p$, $\epsilon = (E_f - E_i)/(1 \text{ Ry})$, and $v_i = [E_i/(1 \text{ Ry})]^{1/2}$. Generally $0.1 \lesssim a_{\text{eik}} \lesssim 0.4$.

We used the eikonal-corrected OBK theory for the rate $\alpha_{\text{CT}} = v_p n_i \sigma_{\text{CT}}$ in all our computations. Figure 1 shows in addition to all the other processes also the charge-transfer-rate coefficient in the 10-eV plasma that stems from the small part (2×10^{-6}) of bound electrons. For comparison Fig. 2 shows the rate coefficients in a cold hydrogen gas of the same density 10^{17} cm^{-3} . The total loss rates in both cases do not differ considerably, but the capture rate drops in the plasma case by about three orders of magnitude.

For large projectile velocities we have approximately

$$\frac{\alpha_{\text{CT}}}{\alpha_{\text{REC}}} \approx 10^9 \frac{Z^2 E_i^{5/2} v_p^{3/2}}{v_p^{11}} \approx 10^9 \frac{E_i^{5/2} Z}{v_p^8 Z_i}, \quad (19)$$

with E_i in Ry and v_p in αc . In cold plasmas with many bound electrons the OBK rate is typically many orders of magnitude larger than the radiative recombination.

D. Solution of the rate equations neglecting dielectronic recombination

The total rates for ionization and recombination without dielectronic recombination are

$$\begin{aligned} \alpha(Z \rightarrow Z+1) &= \sigma_{\text{BEM}}(Z) v_p n_i + \sigma_e(Z) v_r n_e, \\ \alpha(Z \rightarrow Z-1) &= \sigma_{\text{CT}}(Z) v_p n_i + [\sigma_{\text{REC}}(Z) + \sigma_{3\text{BR}}(Z)] v_r n_e. \end{aligned} \quad (20)$$

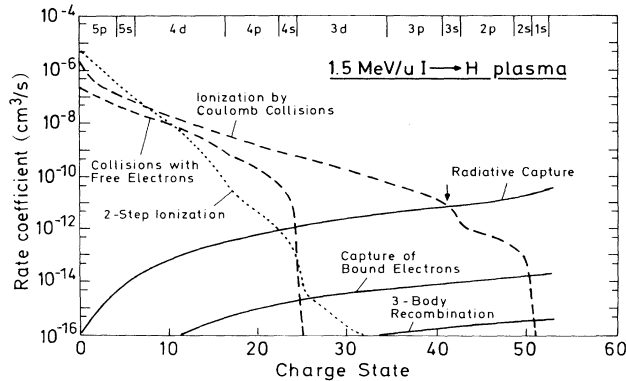


FIG. 1. Rates of electron capture and loss for a 1.5-MeV/u iodine beam in a 10-eV hydrogen plasma with $n_e = 10^{17} \text{ cm}^{-3}$. The intersection between capture and loss curves is close to the equilibrium charge $Z_{\text{eq}}(v_p)$ at constant velocity (arrow).

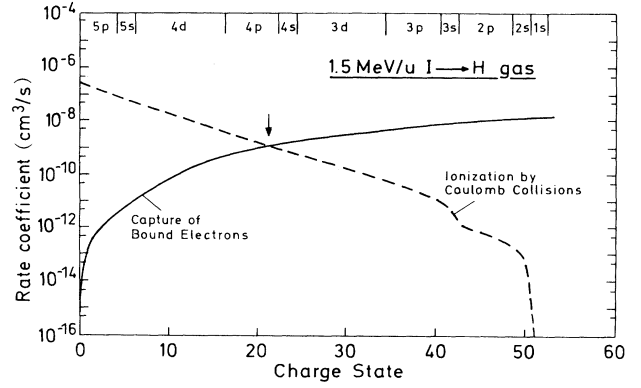


FIG. 2. Rates for 1.5-MeV/u iodine in cold hydrogen gas with $n_e = 10^{17} \text{ cm}^{-3}$. Here the equilibrium charge is about 21 (arrow), thus considerably less than in the plasma case (Fig. 1).

With these rates we solved the rate equations for 1.5 MeV/u iodine ions incident on 10-eV hydrogen plasma with a density of 10^{17} cm^{-3} . Figure 3 shows the charge-state evolution starting from $Z_{\text{eff}} = 0$. Figure 4 shows the equilibrium effective charge Z_{eq} as a function of projectile velocity or ion energy per nucleon calculated from the intersection points of loss and capture rates. For $v_p \leq 10\alpha c$ we find $Z_{\text{eq,hot}} \gg Z_{\text{eq,cold}}$. Only at very high velocities is $Z_{\text{eq,hot}} \lesssim Z_{\text{eq,cold}}$, because, according to Eq. (19), the cross section for charge transfer drops faster at high velocities than the cross section for radiative capture.

Figure 3 also reveals that the equilibrium areal density $\int n_e dl$ (integrated from $Z=0$ to $Z=Z_{\text{eq}}-1$) will be increased by two orders of magnitude. Thus, in order to observe the strong difference of the effective charges in plasma and cold gas in a laboratory experiment it is essential to have a plasma of high enough areal density; in the illustrated case typically about 10^{20} cm^{-2} .

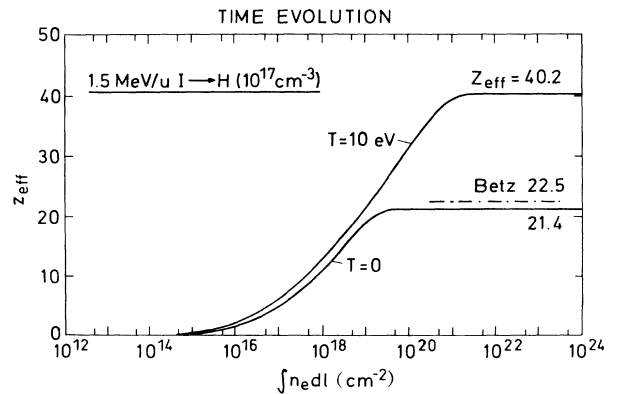


FIG. 3. Time evolution of the effective charge of an iodine beam with 1.5 MeV/u in hydrogen neglecting stopping-power effects. The beam ions have charge zero initially. The dash-dotted line gives the semiempirical value of Betz (Ref. 2) for cold gas.

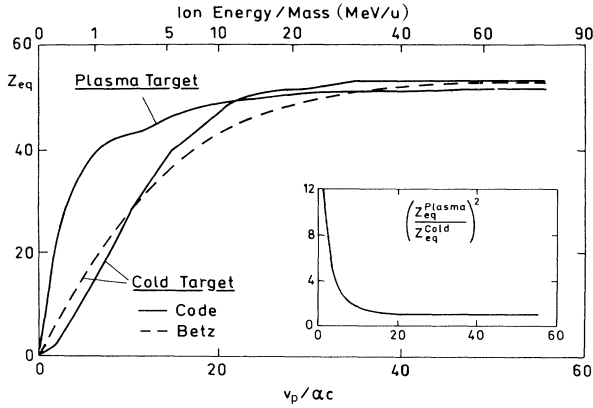


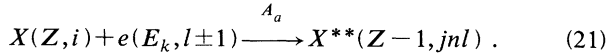
FIG. 4. Equilibrium charge state Z_{eq} for I→H. The target is either 10-eV hydrogen plasma with $n_e = 10^{17} \text{ cm}^{-3}$ or cold hydrogen gas of the same density; dielectronic recombination is not considered.

III. THE SPECIAL ROLE OF DIELECTRONIC RECOMBINATION

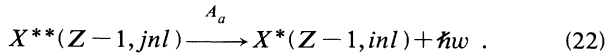
In this section the theory of dielectronic recombination for the case of moving ions in plasma is developed. In addition to autoionization of the captured electron the autoionization of valence electrons is introduced, which becomes important for heavy ions, if the velocity v_p is high enough to excite electrons from inner shells. It is shown that dielectronic recombination (DR) is often the dominant capture mechanism and therefore influences the charge state of fast ions in plasma considerably.

A. The mechanism of dielectronic recombination

Dielectronic recombination is a two-step process in which a free electron with kinetic energy E_k is captured by an ion X of charge Z and the excess energy is transferred to another electron already bound in shell $i \equiv (n_i l_i)$, which will be excited to shell $j \equiv (n_j l_j)$:



The free electron tends to be captured into a highly excited level $n \gg 1$, from where it will usually autoionize by the process Eq. (21) running from right to left (Auger effect with rate A_a). In order to stabilize X^{**} , the energy has to leave the system by other means, for example via a stabilizing radiative decay (with rate A_r):



The photon carries the energy $\hbar\omega = E_j - E_i$. Because of its longer lifetime the higher excited electron remains after the $i \rightarrow j$ transition in the (nl) level, until it finally cascades down to the ground state. Jacobs *et al.*²⁸ examined the possibility of other channels for the radiative decay $j \rightarrow k$, where $n_i < n_k < n_j$. The present work takes only the decay to state i into consideration.

Energy conservation requires $E_k - E_{nl} = E_j - E_i$, where E_k is the kinetic energy of the free electron, E_i the binding energy of the initially bound electron (possibly in an inner shell), and E_j and E_{nl} the energies of the excited states. At first we describe an ion being at rest in a plasma. The number of DR processes per unit volume and time is $n(X^{**})A_r$. This yields a rate coefficient $\alpha_{DR}/n_e = n(X^{**})A_r/n(X)n_e$. Following the principle of detailed balance the total loss of doubly excited ions $n(X^{**})(A_a + A_r)$ is identical with the loss $n_{\text{Saha}}(X^{**})A_a$ in a Saha equilibrium

$$n(X^{**}) = \frac{A_a}{A_r + A_a} n_{\text{Saha}}(X^{**}), \quad (23)$$

where n_{Saha} is given by

$$\frac{n_{\text{Saha}}(X^{**})}{n(X)n_e} = \frac{g(Z-1, jnl \pm 1)}{2g(Z, i)} \frac{h^3}{(2\pi m k_B T)^{3/2}} e^{-E_k/k_B T}. \quad (24)$$

Here, $g(Z, i)$ and $g(Z-1, jnl \pm 1)$ are statistical weights of the states $X(Z, i)$ and $X^{**}(Z-1, jnl \pm 1)$:

$$\begin{aligned} g(Z, i) &\equiv \begin{bmatrix} g_i \\ N_i \end{bmatrix} \begin{bmatrix} g_j \\ N_j \end{bmatrix}, \quad g(Z, j) \equiv \begin{bmatrix} g_i \\ N_i + 1 \end{bmatrix} \begin{bmatrix} g_j \\ N_j + 1 \end{bmatrix}, \\ g(Z-1, jnl) &\equiv \begin{bmatrix} g_i \\ N_i - 1 \end{bmatrix} \begin{bmatrix} g_j \\ N_j + 1 \end{bmatrix} 2(2l+1), \quad (25) \\ g_i &= 2(2l_i + 1), \quad g_j = 2(2l_j + 1). \end{aligned}$$

N_i and N_j are occupation numbers of shells i and j of the ion $X(Z, i)$. Hence the rate for the DR specified by the quantum numbers $(ijnl)$ becomes²⁹

$$\begin{aligned} \alpha_{DR}(ijnl) &= \frac{A_r(j \rightarrow i) A_a(jnl \rightarrow iE_k l \pm 1)}{A_r(j \rightarrow i) + A_a(jnl \rightarrow iE_k l \pm 1)} \\ &\times \frac{g(Z-1, jnl \pm 1)}{2g(Z, i)} \\ &\times \frac{h^3 n_e}{(2\pi m k_B T)^{3/2}} e^{-(E_j - E_i + E_{nl})/k_B T}. \quad (26) \end{aligned}$$

The quantity $A_r A_a / (A_r + A_a)$ is called branching ratio or fluorescence yield.

B. The rates A_r for stabilizing decay and A_a for autoionization

The decay rate A_r for radiative stabilization is given in terms of the Einstein- A coefficient, provided the captured electron in shell n can be treated merely as a ‘‘spectator-electron,’’ which does not influence the $j \rightarrow i$ transition:

$$A_r(j \rightarrow i) = (N_j + 1) \frac{g_i - N_i + 1}{g_j} A_r^{(1)}(j \rightarrow i),$$

where

$$A_r^{(1)}(j \rightarrow i) = \frac{1}{\hbar} \frac{\text{Ry}}{\alpha^3} \left[\frac{E_j - E_i}{1 \text{ Ry}} \right]^2 f^{(1)}(j \rightarrow i). \quad (27)$$

$A_r^{(1)}$ is the absorption rate for one electron and $f^{(1)}(i \rightarrow j)$ the absorption oscillator strength of the $i \rightarrow j$ excitation which we approximate by the results for hydrogen.³⁰

More involved is the calculation of the autoionization rate. The principal of detailed balance yields

$$2(2l+1)g(Z, j)A_a(jnl \rightarrow iE_k l \pm 1) = g(Z, i)2\mathcal{V} \int d^3p \frac{1}{h^3} \frac{v\sigma(iE_k l \pm 1 \rightarrow jnl)}{\mathcal{V}}, \quad (28)$$

where \mathcal{V} is the volume. With the density of states $\rho(E) = 1/(dE/dn) = 1/(2Z^2/n^3 \text{ Ry})$ for the high-lying (nl) state one finds

$$\sigma(iE_k l \pm 1 \rightarrow jnl) = \frac{2Z^2}{n^3} \text{ Ry} \sigma(i\hbar\omega l \pm 1 \rightarrow jnl) \delta(E - \hbar\omega). \quad (29)$$

Due to the δ function Eq. (28) can be evaluated. Following Burgess³¹ and Jacobs *et al.*²⁸ we approximate the capture cross section σ on the right-hand side of Eq. (29) by the excitation cross section

$$\sigma(i\hbar\omega l \pm 1 \rightarrow jnl) \simeq \sigma_{\text{exc}}(iE_k l \pm 1 \rightarrow E_k' l) |_{E_k'=0} \quad (30)$$

for a free-free collision at threshold $E_k = E_j - E_i$. We evaluate the excitation cross section σ_{exc} making use of the Born approximation³²

$$\sigma_{\text{exc}}(iE_k l \pm 1 \rightarrow jE_k' l) = \frac{m^2}{4\pi^2 \hbar^4} \frac{k'}{k} \int d\hat{k}' |\langle \mathbf{k}', j | V_{ji} | \mathbf{k}, i \rangle|^2. \quad (31)$$

The momenta $\hbar k \equiv (2mE_k)^{1/2}$ and $\hbar k' \equiv (2mE_k')^{1/2}$ characterize the wave functions of the free electron before and after the collision, and $\hat{k}' = \mathbf{k}'/|\mathbf{k}'|$. With position vectors \mathbf{r}_1 and \mathbf{r}_2 for the bound and the free electron, respectively, the interaction potential takes the form $V_{ji} = -\mathbf{r}_1 \cdot \mathbf{r}_2 e^2/r_2^3$, and one obtains

$$\alpha_{\text{DR}} = \frac{\hbar^3 n_e}{(2\pi m k_B T)^{3/2}} \sum_i \sum_j \sum_{n,l} N_i \frac{g_j - N_j}{g_j} (2l+1) \frac{A_r^{(1)} A_a^{(1)}}{A_r^{(1)} + A_a^{(1)}} e^{-(E_j - E_i + E_{nl})/k_B T} \quad (36)$$

with the degeneracy factors $g_{i,j} = 2(2l_{i,j} + 1)$.

Finally we need the partial Gaunt-factor \mathcal{G}_l . For the l dependence we use the exponential expression

$$\mathcal{G}_l = N_0 e^{-d(l-l_p)^2} \quad (37)$$

extracted by Gau and Hahn³³ from extensive Hartree-Fock calculations. Here, $l_p = n^{2/3}/\sqrt{1+x}$, $d = \sqrt{1+x}/2.5n$, and $x = n^2 E_k/Z^2 \text{ Ry}$. The \mathcal{G}_l 's are normalized to van Regemorter's value at threshold³⁴

$$f(n) = \sum_l (2l+1) \frac{A_r^{(1)} A_a^{(1)}}{A_r^{(1)} + A_a^{(1)}} \approx \sum_l \frac{(2l+1)e^{-dl^2}}{cn^3(2l+1) + e^{-dl^2}} \approx \int_0^{(n-1)^2} d\xi \frac{1}{cn^3 e^{d\xi} + 1} = (n-1)^2 - \frac{1}{d} \ln \left[\frac{1 + cn^3 e^{d(n-1)^2}}{1 + cn^3} \right] \quad (39)$$

$$\sigma_{\text{exc}}(iE_k l \pm 1 \rightarrow jE_k' l) = \frac{1}{4\pi^2 a_0^2} \frac{k'}{k} \frac{1}{3} |\langle j | \mathbf{r}_1 | i \rangle|^2 \times \int d\hat{k}' \left| \left\langle \mathbf{k}' \left| \frac{\mathbf{r}_2}{r_2^3} \right| \mathbf{k} \right\rangle \right|^2. \quad (32)$$

The interpretation of Eq. (32) is that in the Coulomb field of the atomic electron the colliding electron emits a photon, which then is absorbed in the $i \rightarrow j$ transition. In Eq. (32), $\langle \mathbf{k}' | \mathbf{r}_2/r_2^3 | \mathbf{k} \rangle$ is the matrix element of the Coulomb force for the emission of a photon in a free-free transition, and $\langle j | \mathbf{r}_1 | i \rangle$ is the matrix element of the dipole operator for the bound-bound transition $i \rightarrow j$.

Introducing the partial Kramers-Gaunt factor³²

$$\mathcal{G}_l(k', k) \equiv \frac{kk'\sqrt{3}}{32\pi^4} \int d\hat{k}' \left| \left\langle \mathbf{k}' \left| \frac{\mathbf{r}}{r^3} \right| \mathbf{k} \right\rangle \right|^2 \quad (33)$$

the excitation cross sections reads

$$\sigma_{\text{exc}}(iE_k l \pm 1 \rightarrow jE_k' l) = \frac{8\pi^2}{\sqrt{3}} \frac{1 \text{ Ry}}{E_k} \frac{1 \text{ Ry}}{E_k - E_k'} N_i f(i \rightarrow j) \mathcal{G}_l(k', k). \quad (34)$$

The oscillator strength $f(i \rightarrow j)$ reduces to the one-particle form $f^{(1)}$ according to $f(i \rightarrow j) = N_i (g_j - N_j)/g_j f^{(1)}(i \rightarrow j)$. Hence, the autoionization rate A_a becomes

$$A_a(jnl \rightarrow iE_k l \pm 1) = \frac{g(Z, i)}{g(Z, j)} N_i \frac{g_j - N_j}{g_j} \times A_a^{(1)}(jnl \rightarrow iE_k l \pm 1), \quad (35)$$

where

$$A_a^{(1)}(jnl \rightarrow iE_k l \pm 1) = \frac{8}{\sqrt{3}} \frac{1 \text{ Ry}}{\hbar} \frac{Z^2}{n^3} \frac{1 \text{ Ry}}{E_i - E_j} \frac{1}{(2l+1)} \times f^{(1)}(i \rightarrow j) \mathcal{G}_l(k, k').$$

Most of the weight factors cancel each other and one obtains for the total rate

$$\sum_{l=0}^{n-1} \mathcal{G}_l \approx 0.2 \implies N_0 \approx \frac{0.4}{\sqrt{\pi}} \sqrt{d} (2 - e^{-(0.6/n^{4/3}\sqrt{d})})^{-1}. \quad (38)$$

It is of interest to note the slow convergence of the l sum in Eq. (36). Using $d = (i^{-2} - j^{-2})^{1/2}/2.5$ and $c = 5.9 \times 10^{-7} Z^4 (i^{-2} - j^{-2})^{1/2}$ we obtain in a rough approximation

with the asymptotic forms $f(n) \rightarrow (n-1)^2$ for $n \ll c^{-1/3}$ and $f(n) \rightarrow 1/(dc n^3)$ for $n \gg c^{-1/3}$. The following table shows for a transition $i=2$ to $j=3$ the principal quantum numbers n of those shells where the function $f(n)$ has its maximum (100%), and where it has fallen to 10% or 1% of this maximum value, respectively, as a function of the ion charge Z .

Z	$n_{100\%}$	$n_{10\%}$	$n_{1\%}$
2	8	70	166
10	7	15	33
30	3	9	19

It is seen that the convergence of the dielectronic sum Eq. (39) becomes faster for high- Z ions, though highly excited levels (nl) play an important role even for high-charge states. This behavior is very different from the rigorous $1/n^3$ dependence of radiative electron capture. In the present calculations of the dielectronic rate coefficients shells up to $n=50$ are taken into account. The convergence of the dielectronic sum has important physical consequences, because the captured electron in the highly excited state is very likely to be reionized in secondary collisions due to its long lifetime³⁰ ($T_{nl} \propto n^3 l^2$) and weak binding ($E=Z^2/n^2$ Ry). The rate for this two-step process is proportional to the square of the target density. These density effects are treated in Sec. V.

C. Dielectric recombination for a moving ion

The results of Sec. III B are valid only for an ion at rest relative to the plasma. Here, we need α_{DR} for ions moving with velocity v_p through the plasma. The projectile sees the plasma electrons with a shifted Maxwellian distribution

$$f(\mathbf{v}, \mathbf{v}_p) = n_e \left[\frac{m}{2\pi k_B T} \right]^{3/2} e^{-(m/k_B T)(\mathbf{v} + \mathbf{v}_p)^2}. \quad (40)$$

The dielectronic rate

$$\alpha_{DR} = \int d^3v f(\mathbf{v}, \mathbf{v}_p) \sigma_{DR}(E) |\mathbf{v}| \quad (41)$$

can be easily generalized for this case due to the reso-

nance condition $\sigma_{DR}(E) \propto \delta(E - (E_j - E_i + E_{nl}))$ yielding instead of Eq. (36)

$$\alpha_{DR} = \frac{h^3 n_e}{(2\pi m k_B T)^{3/2}} \sum_i \sum_j \sum_{n,l} N_i \frac{g_j - N_j}{g_j} (2l+1) \times \frac{A_r^{(1)} A_a^{(1)}}{A_r^{(1)} + A_a^{(1)}} F(s, t),$$

where

$$F(s, t) = \frac{e^{-(s-t)^2} - e^{-(s+t)^2}}{4st}$$

with

$$s = \left[\frac{E_j - E_i + E_{nl}}{k_B T} \right]^{1/2}, \quad t = \left[\frac{m v_p^2}{2k_B T} \right]^{1/2}. \quad (42)$$

In the limit $v_p \rightarrow 0$ the pure plasma case is recovered, $F(s, t) \rightarrow \exp[-(E_j - E_i + E_{nl})/k_B T]$. The rate is largest for temperatures with $E_j - E_i \simeq \frac{3}{2} k_B T$ (i.e., $s \simeq (3/2)^{3/2} \gg t$). In the other limit of fast ions in low-temperature plasma ($v_p \gg v_{th}$), the resonance condition is satisfied if $(m/2)v_p^2 \simeq E_j - E_i + E_{nl} \gg k_B T$ (i.e., $s \simeq t \gg 1$). In the latter case the beam probes individual resonance lines of width $k_B T$ as a function of projectile velocity.

D. Autoionization of valence electrons following the excitation of inner-shell electrons

The aim of this section is to extend the treatment for dielectric recombination as outlined above in a direction important for fast heavy ions in plasma. The excitation of bound electrons out of inner shells plays a significant role in the case of high relative velocities between the heavy ion and the free electron. The ions resulting from such an encounter can decay via many autoionization channels. We consider an ion with m electrons in an inner shell i_1 and one valence electron in shell i_2 . If one of the inner-shell electrons is excited in the course of a dielectronic capture $i_1 \rightarrow j$ with $n_j \geq n_{i_2}$, the following processes are possible:

$$X(Z, i_1^m i_2) + e(E_k, l \pm 1) \rightarrow X^{**}(Z-1, i_1^{m-1} i_2 j n l) \rightarrow \begin{cases} X^*(Z-1, i_1^m i_2 n l) + \hbar\omega, \\ X(Z, i_1^m i_2) + e(E_k, l \pm 1), \\ X(Z, i_1^m n l) + e(E_k, l_j \pm 1), \\ X(Z, i_1^m n l) + e(E_k, l_{i_2} \pm 1), \\ X^{**}(Z-1, i_1^m j n l) + \hbar\omega''. \end{cases} \quad (43)$$

Only the upper two paths correspond to the usual dielectronic processes. We use the rate A_a in Sec. III B to approximate the additional autoionization channels of valence electrons; to do so we substitute $n \rightarrow n_j$, or rather $n \rightarrow n_{i_2}$ and $E_i - E_j \rightarrow E(Z-1, i_1^{m-1} i_2 j n l) - E(Z, i_1^m n l)$ in Eq. (35). The branching ratio becomes

$$\frac{A_r A_a}{A_r + A_a} \rightarrow \frac{A_r A_a}{A_r + A_a + A_a^v}. \quad (44)$$

A_a^v stands for the sum of the processes yielding autoionization of valence electrons.

A typical result for the rate coefficient of dielectronic

recombination in fast collisions of heavy ions with electrons is given in Fig. 5 taking into account all the processes described above, as well as the density effects on α_{DR} discussed in Sec. IV. The dependence of α_{DR} on the charge state Z is plotted for a 1.5-MeV/u iodine beam in a fully ionized hydrogen plasma with a temperature 10 eV and a density 10^{20} cm^{-3} . In addition the rate coefficients of radiative electron capture and electron loss of Fig. 1 are shown again for comparison. Similar results for 10-eV hydrogen plasma with a density of 10^{17} cm^{-3} were published in Ref. 7. In contrast to the smooth behavior of radiative capture α_{DR} develops a pronounced shell structure. Dielectronic recombination exceeds radiative electron capture by one to two orders of magnitude in the case of ions with valence electrons in the shells $3s$, $3p$, and $3d$ ($25 \leq Z \leq 42$), corresponding to the dominant $M \rightarrow N$ transition. The sharp edge at $Z=42$ has energetic reasons: for $Z \geq 43$ the plasma electrons do not have enough kinetic energy in the rest frame of the iodine ion to cause an $L \rightarrow M$ transition. The steep slope of α_{DR} from the third to the fourth principal quantum number can be traced back to autoionization A_a^v of valence electrons: for $Z \leq 24$ again M electrons will be excited preferentially, but now the valence electrons of the N shell autoionize. The arrows in Fig. 5 mark the equilibrium charge states Z_{eq} at the intersections between ionization and recombination rates. The value $Z_{eq} \approx 41$, when α_{DR} is ignored (cf. Fig. 1) reduces to $Z_{eq} \approx 29$, when α_{DR} is taken into account. This equilibrium charge is still much higher than the value $Z_{eq} \approx 22$ obtained for cold hydrogen gas of the same density in Fig. 2.

The resonant character of α_{DR} is also reflected in the equilibrium charge state Z_{eq} . The squared charge Z_{eq}^2 as a function of the projectile velocity v_p for an iodine beam in 10-eV hydrogen plasma with density 10^{20} cm^{-3} is depicted as a dashed line in Fig. 6. It shows strong shell

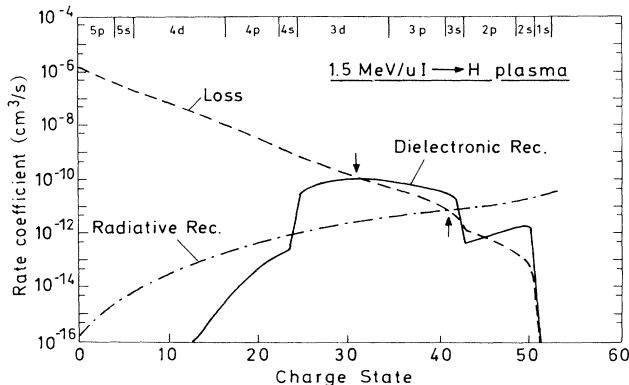


FIG. 5. Rate coefficients for electron loss (dashed curve) and capture (dash-dotted and solid) of 1.5 eV/u iodine ions when penetrating a fully ionized hydrogen plasma of $k_B T = 10 \text{ eV}$ and $n_e = 10^{20} \text{ cm}^{-3}$ as a function of projectile charge state Z . The valence shells corresponding to the various charge states are given at the top of the figure. The arrows mark the equilibrium charge states Z_{eq} with and without dielectronic recombination.

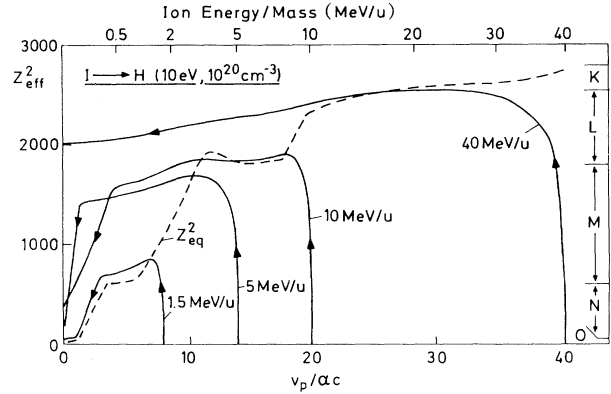


FIG. 6. Evolution of charge states Z_{eff}^2 (solid lines) of iodine ions slowing down in fully ionized hydrogen plasma with $k_B T = 10 \text{ eV}$ and $n_e = 10^{20} \text{ cm}^{-3}$ plotted as a function of projectile velocity v_p in atomic units. Initial energies of the ions are given as parameters on the curves. For comparison the square of the equilibrium charge Z_{eq}^2 is shown as a dashed curve. At the right-hand side, regions of the iodine atomic shells (K , L , etc.) are indicated.

effects, and the plateaus correspond to closed shells. This is evident from the principal shells that are marked at the right axis of the ordinates in Fig. 6. For example imagine an ion with 2 MeV/u and $Z_{eq} = 34$ adiabatically slowing down. It runs through a continuously decreasing series of charge states when the M shell is slowly filled by dielectronic recombination. When the ion still has 1 MeV/u the first electron is captured into the N shell. Further electrons will not be captured because this produces a hole in the M shell with high probability of Auger emission of the N shell valence electron. This explains the plateau between 1 MeV/u and 0.2 MeV/u. Only at energies even smaller the N shell starts to be filled up. For densities above 10^{21} cm^{-3} the shell structure disappears because the density effects (see Sec. IV) quench α_{DR} , so that the dielectronicly lowered equilibrium charge around 0.5 MeV/u and 5 MeV/u increases and Z_{eq}^2 becomes a monotonous, uniformly increasing function of v_p .

IV. DENSITY EFFECTS

The rate coefficients for recombination processes are density independent, as long as conditions for two-body collisions apply. In particular, dielectronic recombination gets considerably reduced at higher densities. This is because the captured electron often ends up in a highly excited level, where it has a long lifetime and is exposed to possible secondary collisions with target particles, which may ionize it before it falls down to the ground state. Such an ionizing secondary collision is the more probable the denser the target material and the higher excited the electron initially is. This density effect cuts back the effective capture rate and is called “quenching”. Lamb³⁵ proposed this effect for cold gaseous targets and Lassen³⁶ provided first experimental evidence that the

effective charge increases slightly when the density of the gas is raised.

A. Reduced rate coefficients subject to various density effects

This work takes the following density effects into account. (i) collisional ionization of simply excited states (collisional quenching); (ii) two-step processes with excitation and subsequent ionization; (iii) dynamical screening of the projectile; (iv) the overlap of wave functions of projectile and target ions.

We do not consider processes of second order, in which at least two electrons get excited simultaneously (Auger processes) or multistep excitations of one electron occur. These events are less likely than (i)–(iv) if the density is not too high. The processes (i) and (ii) vanish at small projectile velocities ($v_p \rightarrow 0$) and low temperatures ($v_{th} \rightarrow 0$). The processes (iii) and (iv) on the other hand remain finite even when the ion is at rest; they are counted under the term “continuum lowering.”

Let P_{nl} be the probability that a simply excited state (nl) originating from the capture of a free electron or from collisional excitation of a bound electron decays radiatively to the ground state before the subsequent collision will ionize the electron. Further let n_g be the principal quantum number of the ground state and n_{max} the quantum number of the highest bound shell in the presence of continuum lowering. Then the reduced, density-dependent recombination rates read

$$\alpha_{REC} = \sum_{n_f=n_g+1}^{n_{max}} \sum_{l_f=0}^{n_f-1} P_{n_f l_f} \alpha(n_f l_f), \quad (45)$$

$$\alpha_{CT} = \sum_{n_i, l_i} \sum_{n_f=n_g+1}^{n_{max}} \sum_{l_f=0}^{n_f-1} P_{n_f l_f} \alpha(n_i l_i, n_f l_f), \quad (46)$$

$$\alpha_{DR} = \sum_{n_i, l_i} \sum_{n_j=n_g+1}^{n_{max}} \sum_{l_j=0}^{n_j-1} P_{n_j l_j} \sum_{n=n_g+1}^{n_{max}} \sum_{l=0}^{n-1} P_{nl} \alpha(ijnl). \quad (47)$$

$$\begin{aligned} \alpha_{exc,e} = & \sum_i \sum_{j=n_g+1}^{n_{max}} \sum_{l=0}^{j-1} \left[v_p^2 + v_{th}^2 \right]^{1/2} n_e \sigma_{exc,e}(iE_k l \pm 1 \rightarrow jE_k l) (1 - P_{jl}) \\ & + \sum_i \sum_{j=n_{max}+1}^{\infty} \sum_{l=0}^{j-1} \left[v_p^2 + v_{th}^2 \right]^{1/2} n_e \sigma_{exc,e}(iE_k l \pm 1 \rightarrow jE_k l). \end{aligned} \quad (50)$$

Here, $\sigma_{exc,e}$ is the free-free excitation cross section according to Eq. (34). The first term on the right-hand side of Eq. (50) describes the excitation into a bound level, whereas the second term allows for direct ionization into a level that due to continuum lowering is no longer bound.

In addition to collisional excitation by electrons there is excitation by the plasma ions with rate $\alpha_{exc,i}$. They are the same as for electron collisions, except for the substitutions³⁷ $\sigma_{exc,e} \rightarrow Z_i^2 \sigma_{exc,e}$ and $(v_p^2 + v_{th}^2)^{1/2} \rightarrow v_p$. The sum $\alpha_{exc,e} + \alpha_{exc,i}$ is shown in Fig. 1 as a dotted curve.

The rate coefficients α_{CT} for charge transfer and α_{REC} for radiative electron capture in Sec. II ask for l_f -averaged input, hence we take $l_f = \text{const} = 1$ in Eqs. (45) and (46). This simplifying assumption is particularly justified in the case of fast collisions for which the capture into $l_f = 1$ subshells dominates.

B. Collisional ionization of simply excited states

The probability P_{nl} reads

$$P_{nl} = \frac{A_{rad}(nl \rightarrow n_g l \pm 1)}{A_{rad}(nl \rightarrow n_g l \pm 1) + A_{coll}(nl, E_k \rightarrow E_k' E_k'')}. \quad (48)$$

A_{rad} is the rate for radiative decay given by the Einstein coefficient Eq. (27) for $l \leq n_g$. If $l > n_g$, the electron can reach the ground level only through a cascade, thus $A_{rad}^{-1}(nl \rightarrow n_g, n_g - 1) = A_{rad}^{-1}(nl \rightarrow l, l - 1) + \sum_{i=1}^{l-n_g-1} A_{rad}^{-1}(l-i, l-i-1 \rightarrow l-i-1, l-i-2)$. The collision rate A_{coll} is given as the sum of ionization rates by Coulomb collisions with background ions in Eq. (7) and free electrons in Eq. (10), evaluated for the state (nl). We give the asymptotic result for large n and v_p (n_i is the ion number density, n is the principal quantum number of the projectile shell)

$$P_{nl}(Z, v_p, n_i) \approx \frac{1}{1 + 5 \times 10^{-18} \frac{Z_i^2 n_i / (1 \text{ cm}^{-3})}{Z^6 v_p / \text{ac}} l^2 n^5}, \quad (49)$$

which may be used for rough estimates of P_{nl} .

C. Two-step processes with excitation and subsequent ionization

The rate for collisional excitation of an electron from the ground state with direct ionization in a second step is given by

D. Continuum lowering by dynamical screening of the projectile

In a plasma of high density the Debye length λ_D describing the correlation between two charges becomes so small that it is comparable to the mean orbital radius of a bound projectile electron $r_n = (n^2/Z_n) a_0$ (Z_n is the effective charge of the projectile core in a distance r_n). In this case the free electrons screen the ion so effectively that the electron in the n th shell is no longer bound. For bound electrons below the continuum limit the following

condition has to be satisfied:³⁸

$$r_n \leq \lambda_D \implies n \leq \left[\frac{Z^2 k_B T}{8\pi} \frac{1}{1 \text{ Ry}} \frac{1}{n_e a_0^3} \right]^{1/4}. \quad (51)$$

Since the dressing of the ion takes time, Eq. (51) is valid only for projectile ions moving very slowly through the plasma or being at rest. At high velocities the screening of the ions is no longer Debye-Hückel-like but much weaker. Qualitatively this corresponds to a larger Debye length. We take this dynamical effect into account using Eq. (10) of Sec. I in paper I: $k_D W(\mu v_p / \sqrt{k_B T / m})$ is equivalent to an effective Debye wave number at velocity v_p . For moderate velocities it is

$$\begin{aligned} |W| &\simeq |1 - (\mu^2 v_p^2 / k_B T / m) \\ &\quad + i\sqrt{(\pi/2)}(\mu v_p / \sqrt{k_B T / m})| \\ &\simeq 1 - \frac{1}{4}(4 - \pi)v_p^2 \mu^2 / k_B T / m. \end{aligned}$$

Averaging this expression with respect to the direction cosine μ we obtain $\langle |W| \rangle \simeq 1 - \frac{1}{12}(4 - \pi)(v_p^2 / k_B T / m)$. This yields instead of Eq. (51)

$$n \leq \left[\frac{Z^2 k_B T}{8\pi} \frac{1}{1 \text{ Ry}} \frac{1}{n_e a_0^3} \right]^{1/4} \left[1 + \frac{1}{12}(4 - \pi) \frac{v_p^2}{k_B T / m} \right]^{1/2}. \quad (52)$$

E. Continuum lowering by overlap of the wave functions of projectile and target ions

Dynamical screening as presented in the preceding subsection is valid for densities $n_e \lambda_D^3 \gg 1$. For even higher densities the ions have approximately spherical volumes of radius $R_0 = [3/(4\pi n_i)]^{1/3}$ at their disposal. A rough criterion for bound states is therefore³⁸

$$r_n \leq R_0 \implies n \leq \left[\frac{3Z^3}{4\pi n_i a_0^3} \right]^{1/6}. \quad (53)$$

In the calculations, we take as the upper limit on n Eq. (52) or Eq. (53) whichever is larger.

V. NONEQUILIBRIUM CHARGE STATES AND STOPPING POWERS IN DENSE PLASMA

In the following the stopping of heavy ions in dense plasma is calculated, based on the results of paper I on the plasma physics of the stopping process, but now with full account of the charge-state evolution of the heavy-ion projectile using the ionization and recombination rates discussed in the present paper. It is shown that strongly enhanced nonequilibrium charge states are typical for heavy-ion stopping in plasma.

In solid-state or gaseous cold matter beam ions acquire their effective equilibrium charge Z_{eq} after a short equilibration phase. The typical time for recombination $\tau_{\text{REC}} = 1/(\alpha n_e)$ (α is the recombination rate coefficient) is much shorter than the time $\tau_{\Delta E} = -1/(dv_p/dx)$ for stop-

ping the ion. The time dependence of the effective charge is therefore exclusively determined by the local velocity of the beam ions: $Z_{\text{eff}}(v(t), t) = Z_{\text{eq}}(v(t))$. However, in a plasma it is possible that $\tau_{\text{REC}} \gtrsim \tau_{\Delta E}$ because of the drastically reduced recombination rate, the higher equilibrium charge Z_{eq} and the larger Coulomb logarithm. The recombination of free electrons then no longer keeps pace with the stopping process, hence $Z_{\text{eff}}(v(t), t) \gg Z_{\text{eq}}(v(t))$. This yields a further shortening of the ion range.

The occurrence of nonequilibrium charge states complicates the stopping process since the values of Z_{eff} and dE/dx along the stopping path depend on the full stopping history and not just on the local velocity. It is therefore difficult to map out the solution over a larger parameter region. We rather give some illustrative examples closely related to recent experiments and experiments planned in the near future. Also some results relevant for inertial confinement fusion driven by heavy ion beams will be shown.

A. Stopping power of partially ionized plasma

The electron stopping power

$$-\frac{dE}{dx} = \frac{4\pi e^4 Z_{\text{eff}}^2}{m v_p^2} N_i L \quad (54)$$

is chosen in standard form proportional to Z_{eff}^2 and linear in the target ion density N_i . In a target plasma with atomic number Z_i and effective charge q_i the stopping number per ion

$$L = q_i L_f + (Z_i - q_i) L_b \quad (55)$$

is composed of the free-electron contribution

$$\begin{aligned} L_f &= G(v_p / \sqrt{k_B T / m}) \ln(\lambda_D k_{\text{max}}) \\ &\quad + H(v_p / \sqrt{k_B T / m}) \ln(v_p / \sqrt{k_B T / m}) \end{aligned} \quad (56)$$

with the functions

$$G(x) = \text{erf}(x/\sqrt{2}) - \sqrt{2/\pi} x \exp(-x^2/2) \quad (57)$$

$$H(x) = -x^3 \exp(-x^2/2) / (3\sqrt{2\pi} \ln x) + x^4 / (x^4 + 12),$$

the Debye length $\lambda_D = (k_B T / 4\pi e^2 n_e)^{1/2}$ and the momentum cutoff

$$k_{\text{max}} = \min\{m(v_p^2 + v_{\text{th}}^2) / |Z_{\text{eff}}| e^2, 2m v_p / \hbar\} \quad (58)$$

as derived in paper I, and the contribution from bound electrons

$$L_b = \ln \left[\frac{2m v_p^2}{\bar{I}} \right] \quad (59)$$

according to Bethe's theory.³⁹ In the present calculations the average ionization potentials for the partially ionized target ions \bar{I} are taken from Mehlhorn.⁴ For small ion velocities v_p , Bethe's stopping power $(dE/dx)_{\text{Bethe}}$ becomes invalid and is replaced by the expression of Linhard, Scharff, and Schiøtt⁴⁰ (LSS model)

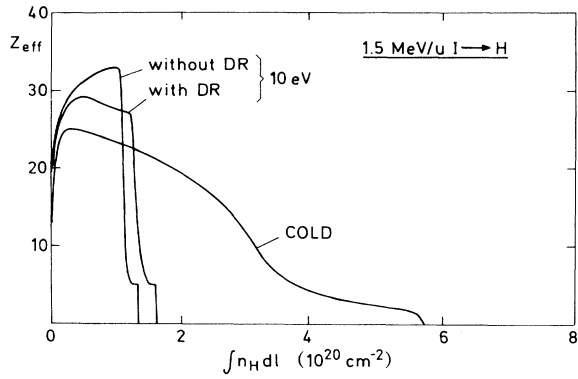


FIG. 7. Effective charge Z_{eff} of an iodine projectile with initial energy 1.5 MeV/u slowing down in hydrogen with a density $n_{\text{H}} = 10^{20} \text{ cm}^{-3}$ plotted vs range $\int n_{\text{H}} dl$. The curves refer to 10 eV plasma with and without account of DR and to cold gas.

$$\left(\frac{dE}{dx} \right)_{\text{LSS}} = C_{\text{LSS}} E \quad (60)$$

with $E = M_p v_p^2 / 2$. The parameter C_{LSS} depends on atomic numbers and atomic masses of both projectile and target ions. The total stopping power is calculated using a smooth interpolation between the Bethe and LSS expressions for bound electron stopping

$$\frac{dE}{dx} = \frac{(dE/dx)_{\text{Bethe}}}{[1 + (dE/dx)_{\text{Bethe}}^2 / (dE/dx)_{\text{LSS}}^2]^{1/2}} + \left(\frac{dE}{dx} \right)_{\text{free}}, \quad (61)$$

with $L_b = \ln(1 + 2mv_p^2/\bar{I})$ instead of Eq. (59). In addition we included the shell corrections in the stopping power according to Mehlhorn⁴ with a simple fit using the empirical values given by Ziegler.⁴¹ However, for the final results neither the LSS model nor the shell correction play an important role. Equations (54)–(61) define the stopping power used in the following to calculate the energy loss of heavy ions in hydrogen, lithium, and gold plasma.

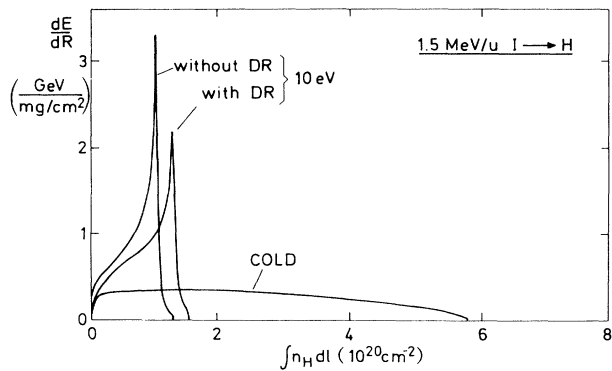


FIG. 8. Stopping powers vs range for the same cases as in Fig. 7.

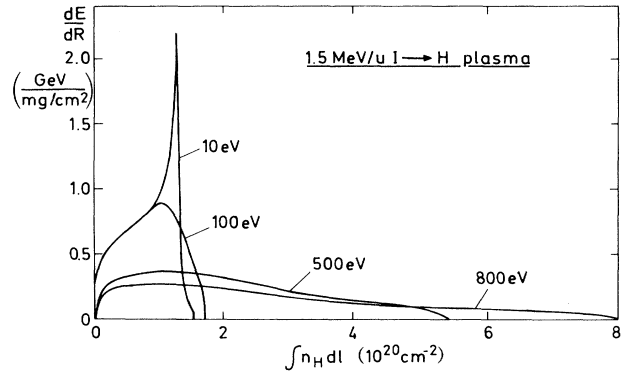


FIG. 9. Stopping powers vs range for 1.5-MeV/u iodine ions on H plasma with $n_e = 10^{20} \text{ cm}^{-3}$ and different temperatures given as labels.

B. Stopping of iodine ions in hydrogen plasma

As a first example to illustrate the effects of range shortening in plasma, nonequilibrium charge states, and dielectronic recombination, results are shown in Figs. 6–10 on the stopping of iodine ions in fully ionized hydrogen plasma of 10-eV temperature and a density of $n_e = 10^{20} \text{ cm}^{-3}$. This density is chosen in between densities presently achieved with Z-pinch devices and used for experiments on heavy-ion interaction with plasma on the one hand, and densities of beam generated plasmas available in the near future on the other hand.¹²

The nonequilibrium evolution of charge states is seen in Fig. 6. The square of the charge state, required in the stopping power Eq. (54), is plotted versus projectile veloc-

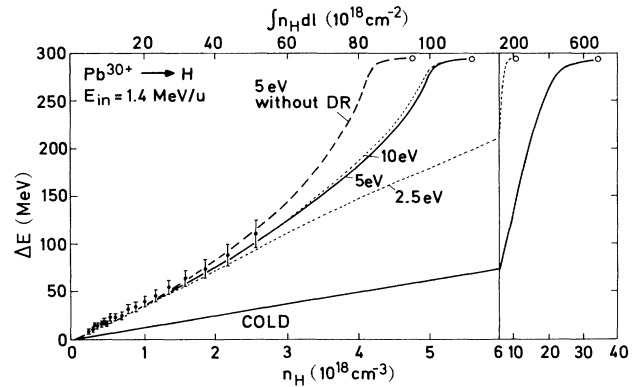


FIG. 10. Energy loss ΔE of Pb projectiles with initial charge state $Z_{\text{in}} = 30$ and initial energy 1.4 MeV/u after passing a 20 cm long column of hydrogen plotted as function of density n_{H} or the corresponding areal density $\int n_{\text{H}} dl$ (upper horizontal axis). Curves for cold H gas and for H plasma of 2.5 , 5 , and 10 eV temperature are given as well as for 5 eV without account of DR and are compared with the experimental data of Ref. 11. Complete stopping is marked by a circle at the end of the curves. Note the change of scales on the right-hand side.

ity v_p . The equilibrium value Z_{eq}^2 depicted as a dashed line is a function of v_p only; it was discussed in Sec. III D. The solid lines give the charge-state evolution of the corresponding nonequilibrium calculation in which Z_{eff} is calculated from the time-dependent rate equations simultaneous with the energy loss. The projectiles are assumed to be injected into the plasma as neutral iodine atoms and their charge state then evolves in the direction indicated by the arrows. It is seen that the ions run through remarkably different charge-state sequences depending on their initial energy given as label in Fig. 6. After fast initial ionization the charge states typically stay on a plateau high above equilibrium values. The higher the plateau value is, the faster the stopping and the shorter the time left for recombination. Whereas Z_{eff} of the 1.5-MeV/u projectile evolves still close to the equilibrium curve, the 40-MeV/u projectile loses its energy so fast that recombination is lagging behind and the ion comes to rest with $Z_{\text{eff}} \approx 45$. It recollects the missing electrons only after complete stopping. Such highly charged ions at rest in very dense and relatively cold plasma are rather unique objects and should be of considerable interest for spectroscopic studies.

The charge-state distribution along the stopping range $\int n_H dl$ is plotted in Fig. 7 for 1.5 MeV/u I ions incident on a hydrogen target again with a density of $n_H = 10^{20} \text{ cm}^{-3}$. Profiles for 10-eV plasma are compared with the case of a cold target gas; the stopping range in plasma is shorter by a factor 3. The shortening is a consequence of three temperature-dependent effects reinforcing each other: (1) increase of the Coulomb logarithm $\Lambda_{\text{plasma}} > \Lambda_{\text{gas}}$; (2) increase of the equilibrium charge $Z_{\text{eq,plasma}} > Z_{\text{eq,gas}}$; (3) further increase by nonequilibrium effects $Z_{\text{eff}}(v(t), t) \gg Z_{\text{eq}}(v(t))$. Also shown in Fig. 7 is the effect of DR which reduces the charge state (compare Fig. 5) and therefore increases the range. The corresponding distribution of the stopping power dE/dR versus the range is shown in Fig. 8. Whereas a pronounced peak (Bragg peak) is seen at the end of the range in the plasma curves with a maximum of $dE/dR = 2 \text{ GeV}/(\text{mg}/\text{cm}^2)$, the deposition profile is completely flat for the cold gas with an average $dE/dR \approx 0.3 \text{ GeV}/(\text{mg}/\text{cm}^2)$. This is a consequence of both, the different charge-state behavior and the different Coulomb logarithms for a gas or a fully ionized plasma. The change of the deposition profile with plasma temperature is shown in Fig. 10; for high temperatures when the thermal electron velocity exceeds the projectile velocity, the plasma functions $G(x)$ and $H(x)$ in Eq. (56) decrease and range lengthening occurs.

C. Energy loss and charge state of Pb ions passing a hydrogen plasma

In this section experimental results on the energy loss ΔE of Pb^{30+} ions, having an initial energy of $E_{\text{in}} = 1.4 \text{ MeV}/u$ (which corresponds to 291.2 MeV total energy) and passing through a hydrogen plasma, are compared with calculated results as shown in Fig. 10. The plasma column of 20-cm length was generated in a Z pinch, and measurements were made at different plasma densities

during the compression phase of the pinch. The largest energy loss measured was about 110 MeV at a density of $2.5 \times 10^{18} \text{ cm}^{-3}$. The data points in Fig. 10 are in good agreement with the theoretical curves corresponding to the full model description developed in this paper and a plasma temperature of 5–10 eV. The plasma data are about a factor of 3 larger than the values for the cold gas. This confirms the prediction of enhanced stopping in plasma. Also the curve for 2.5 eV is clearly below the empirical points, whereas the 5-eV curve obtained without accounting for dielectronic recombination would also be consistent with the data. The measurements should be carried to higher densities to obtain a clear discrimination for dielectronic recombination effects. According to the calculations the Pb ions would be stopped completely at a plasma density of $5.6 \times 10^{18} \text{ cm}^{-3}$ corresponding to a stopping range of $1.1 \times 10^{20} \text{ cm}^{-2}$. This range is roughly a factor of 6 smaller than the range in cold gas.

In these experiments the incident Pb ions have a charge state $Z_{\text{in}} = 30+$. The charge state after passing the 20-cm long plasma column will be measured in future experiments. The corresponding calculated values are shown in Fig. 11 for the same cases as in Fig. 10. The charge state is rising to values above 30 for the plasma cases except at high densities when the ion has almost come to rest. Without DR values up to 40 are obtained, five units more than with DR. On the other hand, the charge state is falling by five or six units in the case of a cold H gas with densities up to $5 \times 10^{18} \text{ cm}^{-3}$.

In Figs. 12 and 13 an extension of Figs. 10 and 11 is given to Pb^{30+} ions with a higher initial energy $E_{\text{in}} = 6 \text{ MeV}/u$. At this ion energy, plasma densities up to $4 \times 10^{19} \text{ cm}^{-3}$ can be explored with the 20-cm Z pinch. Results for 5-eV plasma and for cold gas are compared. The relative difference of ΔE in plasma and gas (though not the absolute one) is considerably reduced for these higher energies. The same is true for Z_{eff} . What may be more interesting to measure in future experiments is the

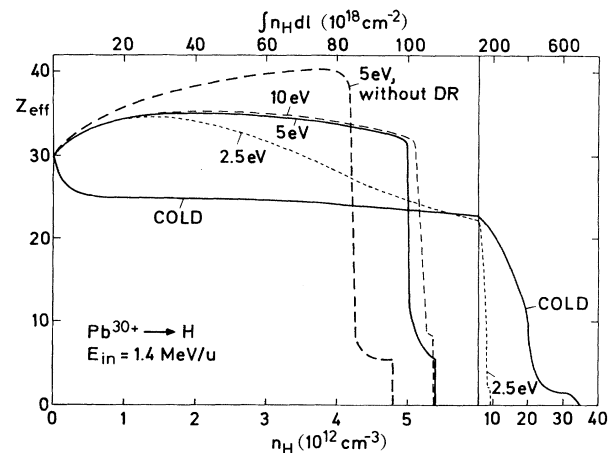


FIG. 11. Effective charge Z_{eff} after passing a 20-cm long column of hydrogen for the same cases as in Fig. 10.

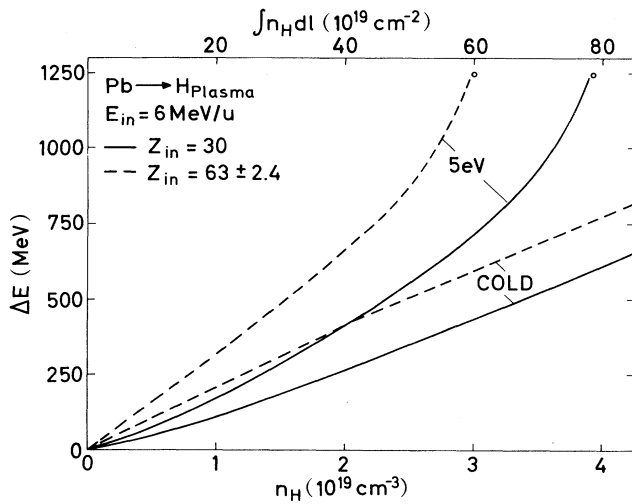


FIG. 12. Energy loss ΔE of Pb projectiles as in Fig. 10, but for an initial energy of $E_{in} = 6$ MeV/u and an initial charge state $Z_{in} = 30$ (solid) or a charge-state distribution $Z_{in} = 63 \pm 2.4$ (dashed) corresponding to the equilibrium distribution of 6 MeV/u Pb behind a stripper foil. Curves for cold H gas and for 5-eV H plasma are compared.

sensitivity of ΔE and Z_{eff} on the charge state Z_{in} of the incident ion. Results for $Z_{in} = 63+$, corresponding to the charge state of 6-MeV/u Pb ions after a solid stripper foil, are shown in Figs. 12 and 13 in addition to those for $Z_{in} = 30+$.

D. Cases relevant to heavy-ion beam ICF

The effects discussed above are also important for heavy-ion-induced ICF, although in this case the beam-target interaction is characterized by higher projectile en-

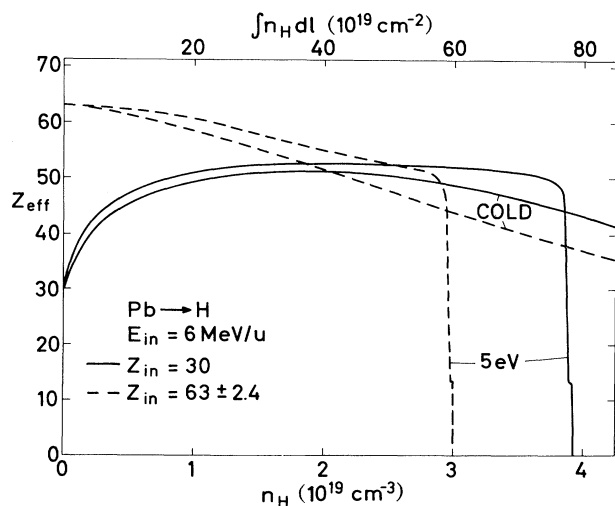


FIG. 13. Effective charge Z_{eff} as in Fig. 11 for the same cases as in Fig. 12.

ergies and higher plasma temperatures and densities (see e.g., Ref. 42). For illustration we take typical parameters from the HIBALL reactor study:⁴³ $E_0 \approx 50$ MeV/u, $k_B T \approx 300$ eV, $n_e \approx 10^{21} - 10^{23}$ cm⁻³. It is assumed that a powerful beam of Bi ions directly drives a spherical fusion pellet. The ions are stripped to $Z_{eff} = 80$ in a high-Z tamper layer at the outer surface of the pellet. They then plunge with 30 MeV/u into a lithium absorber layer where they are finally stopped. The charge-state evolution as a function of projectile velocity is shown in Fig. 14 for this final stopping phase, assuming that the lithium has been heated to 300 eV and has a uniform ion density of 10^{21} cm⁻³ (compare Ref. 44). Results for a density of 10^{17} cm⁻³ and the equilibrium curve Z_{eq}^2 are also shown for comparison. It is seen that, even for this high plasma density, the projectile charge states develop at a level considerably above the equilibrium values though lower than for the 10^{17} cm⁻³ case due to the density effects discussed in Sec. IV and the smaller Debye length in Eq. (56).

Actual deposition profiles of the 30-MeV/u Bi ions in the lithium layer are shown in Fig. 15. Their range of $R = 70$ mg/cm² in cold solid lithium reduces to $R = 44$ mg/cm² or 63% of the cold range, for the lithium plasma with $T = 300$ eV and $\rho = 0.1$ g/cm³. About 50% of the reduction are due to a larger Coulomb logarithm, and the other 50% stem from enhanced projectile charge states. In plasma a Bragg peak forms at the end of the range with a maximum stopping about three times larger than in the cold target. Another range shortening of a factor 2 and the buildup of a huge Bragg peak would occur for a much lower density of $1 \mu\text{g}/\text{cm}^3$, which is of relevance for basic experiments but not in the context of ICF.

The last example given in Fig. 16 is the case of the 30 MeV/u I ions incident on a gold target of $\frac{1}{10}$ solid density. Such high-Z targets play a role for converting ion-

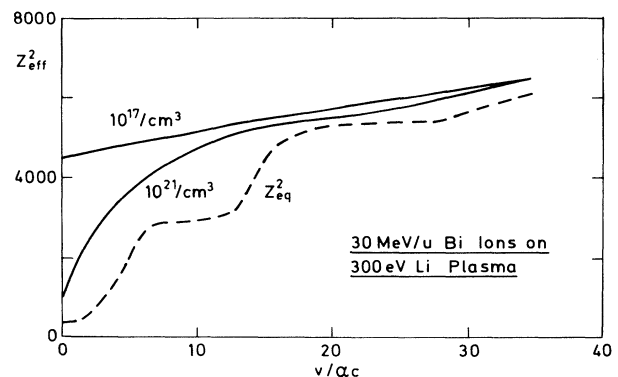


FIG. 14. The square of the effective charge of Bi ions on their path through Li plasma with temperature 300 eV and densities $n_{Li} = 10^{17}$ cm⁻³ and 10^{21} cm⁻³. The ions start out as Bi^{80+} with $E_{in} = 30$ MeV/u ($v_p = 34.7\alpha c$) and slow down along the solid lines from right to left. At the end ($v_p = 0$) they are in charge state $Z_{eff} = 67$ or $Z_{eff} = 31$ depending on the plasma density. The dashed curve shows the equilibrium charge, which corresponds to $n_{Li} = 10^{17}$ cm⁻³; it depends only slightly on density.

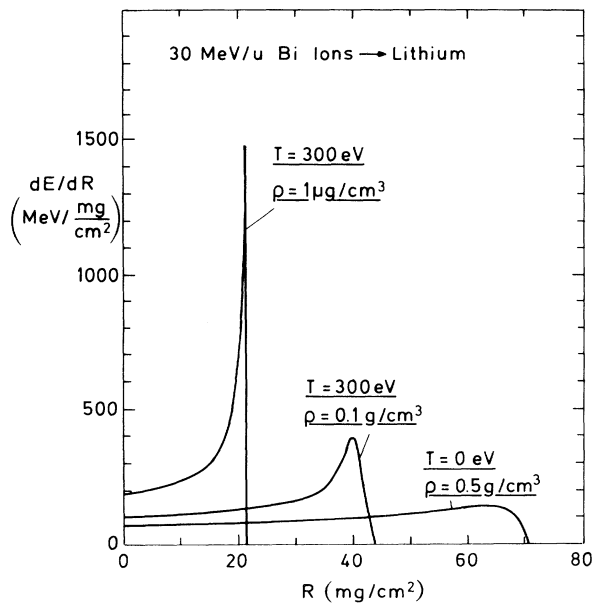


FIG. 15. Stopping power of Bi ions in Li plasmas vs range for three different combinations of densities and temperatures.

beam energy into soft thermal x rays⁴⁵ and are important for x ray driven ICF (see e.g., Ref. 12). Again considerable range shortening is obtained from $R = 180 \text{ mg/cm}^2$ for the cold target to $R = 125 \text{ mg/cm}^2$ for the plasma target at a working temperature of 300 eV, and the peak stopping power at the end of the range rises by a factor of

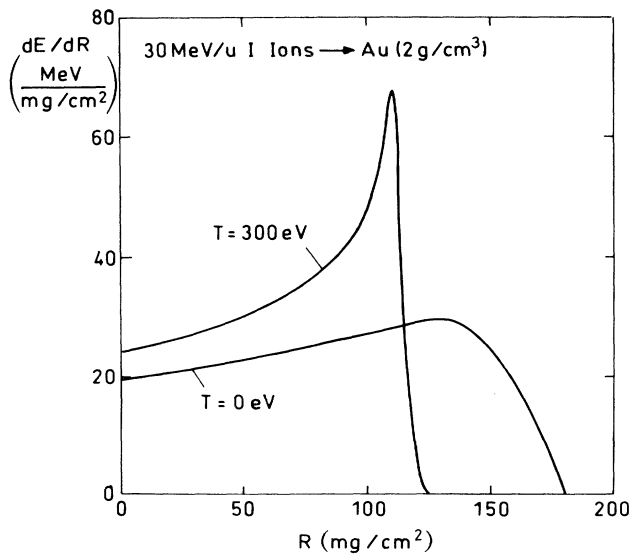


FIG. 16. The stopping power of 30 MeV/u iodine ions in gold plasma of $\frac{1}{10}$ solid-state density and 300 eV temperature in comparison with the stopping power in cold gold of the same density.

2 to $dE/dR = 70 \text{ MeV}/(\text{mg}/\text{cm}^2)$. According to the Saha equation the gold ions in the plasma case were assumed to be in charge state 36+ and the mean ionization potential \bar{I} was obtained from the cold value using the scaling proposed by Mehlhorn.⁴

VI. CONCLUSIONS

The stopping power of heavy ions in dense plasma has been investigated with the attention focused on the projectile effective charge. As a general result, enhanced energy loss and corresponding range shortening of ions slowing down in ionized target matter is confirmed. The major factors for enhancement of $dE/dR \propto Z_{\text{eff}}^2 \ln \Lambda$ are the following.

(1) Projectile energy is more efficiently transferred to free plasma electrons than to the bound electrons in cold material; this leads to an increase of the Coulomb logarithm $\ln \Lambda$.

(2) The charge states Z_{eff} of heavy ions are higher in ionized stopping material due to reduced electron recombination. This is because the large rates for the exchange of bound electrons with the projectile become ineffective with increasing target ionization.

Both mechanisms have been described before in a number of papers. The key finding of the present paper is the identification of high nonequilibrium charge states along the stopping path. The time scales for the charge-changing processes and for energy loss become comparable in plasma. This is a qualitatively new situation and in contrast to heavy-ion stopping in condensed matter, where charge equilibration occurs faster and the projectile charge states are given locally by the equilibrium values $Z_{\text{eq}}(v_p)$ depending on the instantaneous velocity of the projectile v_p . For typical plasma parameters, it now turns out that $Z_{\text{eff}} \gg Z_{\text{eq}}$, in particular, near the end of the ion range. This further shortens the range and leads to rather pronounced Bragg peaks with peak stopping powers enhanced by factors 2 and more due to nonequilibrium effects. It should be noticed that these effects are strongest for relatively low target densities ($n_e < 10^{21} \text{ cm}^{-3}$) and for projectile energies of 1–10 MeV/u, where most of the ionization takes place. Some important conclusions can be drawn.

A. Theory

The details of heavy-ion stopping in plasma are by far more complex than in condensed matter because the effective charge of the projectile is no more a unique function of its local velocity (as given, e.g., by the Betz formula for gas targets), but depends in a nonlocal way on the prehistory of the charge-state evolution and strongly on the initial charge state of the incident heavy ion. Rate calculations following this evolution are complicated by the fact that dielectronic recombination, a two-step process sensitively depending on atomic structure, becomes dominant in highly ionized targets.

B. Experiments

Recent experiments on heavy-ion energy loss in fully ionized hydrogen plasma have been shown to be in good agreement with the theoretical treatment presented in this paper and impressively display the effect of range shortening in plasma. These experiments should be extended; measurements of the charge state after passing the plasma as a function of the incident would give specific information on the nonequilibrium charge-state evolution.

Of course, the most sensitive test of the physics discussed in this paper would be to detect the projectile radiation, spatially resolved along the stopping path, in particular, close to the end of the range in cases where the heavy ion is stopped completely.⁴⁶ The x-ray spectra of recombining electrons cascading down in the highly ionized projectiles should give abundant information not only about charge-state sequences, but also about the inner dynamics of very dense plasma which is hardly investigated so far. The decelerating heavy ion as a plasma probe may open a fascinating new field of dense plasma spectroscopy. The high-current heavy-ion beams, expected to be available, e.g., at the Gesellschaft für Schwerionenforschung (GSI) in the near future, may be the tool to make this kind of spectroscopy possible.

C. ICF applications

Concerning heavy-ion driven inertial fusion, the results of this paper seem to be of minor importance. What matters most for fusion pellets is the ion range. As long as the range becomes shorter by heating the target, it is the cold range which determines the extension of the beam deposition layer. Also, taking the heavy-ion energy of 50 MeV/u chosen in the HIBALL reactor study as a reference value, the nonequilibrium charge states discussed in this paper play a role only at the end of the range and the additional range shortening will be 10–20% at most. However, the increase of energy deposition in the Bragg peak region may be of importance for converting beam energy into soft X rays⁴⁵ and therefore for heavy-ion fusion using indirect drive.

ACKNOWLEDGMENTS

The authors acknowledge first of all the scientific support of R. Arnold during the early phases of this work. They also thank H.-D. Betz, C. Deutsch, D. H. H. Hoffmann, S. Witkowski, and Z. Zinamon for many helpful discussions. This work was supported in part by the Bundesminister für Forschung und Technologie (Bonn, Federal Republic of Germany) and by EURATOM.

-
- ¹Th. Peter and J. Meyer-ter-Vehn, preceding paper, Phys. Rev. A **43**, 1998 (1991).
- ²H.-D. Betz, in Appl. At. Coll. Phys. **4**, 1 (1983).
- ³V. S. Nikolaev and I. S. Dmitriev, Phys. Lett. **28A**, 278 (1968).
- ⁴T. A. Mehlhorn, J. Appl. Phys. **52**, 6522 (1981).
- ⁵M. M. Basko, Fiz. Plazmy **10**, 1195 (1984) [Sov. J. Plasma Phys. **10**, 689 (1984)].
- ⁶E. Nardi and Z. Zinamon, Phys. Rev. Lett. **49**, 1251 (1982).
- ⁷Th. Peter, R. Arnold, and J. Meyer-ter-Vehn, Phys. Rev. Lett. **57**, 1859 (1986).
- ⁸R. Bimbot, S. Della-Negra, M. Dumail, D. Gardes, M. F. Rivet, C. Fleurier, A. Sanba, B. Dumax, D. H. H. Hoffmann, K. Weyrich, J. Jacoby, H. Wahl, C. Deutsch, and G. Maynard, in *Laser Interaction and Related Plasma Phenomena*, edited by H. Hora and G. H. Miley (Plenum, New York, 1988), Vol. 8, p. 665.
- ⁹D. H. H. Hoffmann, K. Weyrich, H. Wahl, Th. Peter, J. Meyer-ter-Vehn, J. Jacoby, R. Bimbot, D. Gardes, M. F. Rivet, M. Dumail, C. Fleurier, A. Sanba, C. Deutsch, G. Maynard, R. Noll, R. Haas, R. Arnold, and S. Maurmann, Z. Physik A **30**, 339 (1988).
- ¹⁰K. Weyrich, D. H. H. Hoffmann, J. Jacoby, H. Wahl, R. Noll, R. Haas, H. Kunze, R. Bimbot, D. Gardes, M. F. Rivet, and C. Deutsch, Nucl. Instrum. Methods A **278**, 52 (1989).
- ¹¹K. G. Dietrich, K. Mahrt-Olt, J. Jacoby, E. Boggasch, M. Winkler, B. Heimrich, and D. H. H. Hoffmann, Laser Part. Beams **8**, 583 (1990).
- ¹²J. Meyer-ter-Vehn, Plasma Phys. Control. Fusion **31**, 1613 (1989).
- ¹³J. C. Slater, Phys. Rec. **36**, 57 (1930).
- ¹⁴M. Gryzinski, Phys. Rev. A **138**, 305 (1965); **A38**, 322 (1965); **138**, 336 (1965).
- ¹⁵J. H. McGuire and P. Richard, Phys. Rev. A **8**, 1374 (1973).
- ¹⁶G. I. Bell, Phys. Rev. **90**, 548 (1953).
- ¹⁷W. Lotz, Z. Physik, **206**, 205 (1967).
- ¹⁸Ya. B. Zel'dovich and Yu. P. Raizer, *Physics of Shock Waves and High-Temperature Hydrodynamic Phenomena* (Academic Press, New York, 1966), Vol. I, pp. 406ff.
- ¹⁹D. H. Menzel and C. L. Pekeris, Mon. Not. Roy. Astron. Soc. **96**, 77 (1935).
- ²⁰D. H. Menzel, Astrophys. J. **85**, 330 (1937).
- ²¹L. Spitzer, Jr., Astrophys. J. **107**, 7 (1948).
- ²²L. P. Pitaevskii, Zh. Eksp. Teor. Fiz. **42**, 1326 (1962) [Sov. Phys.—JETP **15**, 919 (1962)].
- ²³A. V. Gurevich and L. P. Pitaevskii, Zh. Eksp. Teor. Fiz. **46**, 1281 (1964) [Sov. Phys.—JETP **19**, 870 (1964)].
- ²⁴J. R. Oppenheimer, Phys. Rev. **31**, 349 (1928).
- ²⁵H. C. Brinkmann and H. A. Kramers, Proc. Ned. Akad. Wet. **33**, 973 (1930).
- ²⁶R. M. May, Phys. Rev. A **136**, 669 (1964).
- ²⁷J. K. M. Eichler and F. T. Chan, Phys. Rev. A **20**, 104 (1979); J. K. M. Eichler, A. Tsuji, and T. Ishihara, *ibid.* **23**, 2833 (1981).
- ²⁸V. L. Jacobs, J. Davis, P. C. Kepple, and M. Blaha, Astrophys. J. **211**, 605 (1977).
- ²⁹D. R. Bates and A. Dalgarno, in *Atomic and Molecular Processes*, edited by D. R. Bates (Academic, New York, 1962).
- ³⁰H. A. Bethe and E. E. Salpeter, *Quantum Mechanics of One- and Two-Electron Atoms* (Springer, Berlin, 1957).
- ³¹A. Burgess, Astrophys. J. **139**, 776 (1964).
- ³²M. J. Seaton, in Ref. 29.
- ³³J. N. Gau and Y. Hahn, Phys. Lett. **68A**, 197 (1978).
- ³⁴H. Van Regemorter, Astrophys. J. **136**, 906 (1962).
- ³⁵W. E. Lamb, Phys. Rev. **58**, 696 (1940).
- ³⁶N. O. Lassen, Mat. Fys. Medd.-K. Dan. Vidensk. Selsk. **26** (5) (1951); **26** (12) (1951).

- ³⁷N. F. Mott and H. S. W. Massey, *The Theory of Atomic Collisions* (Clarendon, Oxford, 1965).
- ³⁸R. M. More, in *Applied Atomic Collision Physics*, edited by C. F. Barnett, M. F. A. Harrison, H. S. W. Massey, E. W. McDaniel, and B. Bederson (Academic, New York, 1984), Vol. II.
- ³⁹H. Bethe, *Ann. Phys. (N.Y.)* **5**, 325 (1930).
- ⁴⁰J. Linhard, M. Scharff, and H. S. Schiøtt, *Kgl. Danske Videnskab. Selskab., Mat. Fys. Medd.* **33** (14) (1963).
- ⁴¹J. F. Ziegler, *Stopping Cross Sections for Energetic Ions in All Elements* (Pergamon, New York, 1980), Vol. 5.
- ⁴²R. C. Arnold and J. Meyer-ter-Vehn, *Rep. Prog. Phys.* **50**, 559 (1987).
- ⁴³D. Böhne, I. Hofmann, G. Kessler, G. L. Kulcinski, J. Meyer-ter-Vehn, U. von Möllendorf, G. A. Moses, R. W. Müller, I. N. Sviatoslavsky, D. K. Sze, and W. Volgelsang, *Nucl. Engin. Design* **73**, 195 (1982).
- ⁴⁵M. Murakami and J. Meyer-ter-Vehn, *X-Ray Sci. Technol.* **2**, 127 (1990).
- ⁴⁶During the preparation of this manuscript we learned about similar work by E. Nardi and Z. Zinamon, *Laser Part. Beams* **8**, 635 (1990).